

Solar Activity Phases and Intermediate-degree Mode Frequencies

Kiran Jain, S. C. Tripathy and F. Hill

*Global Oscillation Network Group, National Solar Observatory, 950 N Cherry Avenue,
Tucson, AZ 85719, USA*

kjain@noao.edu, stripathy@noao.edu, fhill@noao.edu

ABSTRACT

We analyze intermediate degree p -mode eigenfrequencies measured by GONG and MDI/SOHO over a solar cycle to study the source of their variability. We carry out a correlation analysis between the change in frequencies and several measures of the Sun's magnetic activity that are sensitive to changes at different levels in the solar atmosphere. The observations span a period of about 12 years starting from mid-1996 (the minimum of cycle 23) to early-2008 (near minimum of cycle 24), corresponding to a nearly complete solar activity cycle. We demonstrate that the frequencies do vary in phase with the solar activity indices, however the degree of correlation differs from phase to phase of the cycle. During the rising and declining phases, the mode frequency shifts are strongly correlated with the activity proxies whereas during the high-activity period, the shifts have significantly lower correlation with all activity proxies, except for the 10.7-cm radio flux. In particular, the proxies that are only influenced by the variation of the strong component of the magnetic field in the photosphere have a much lower correlation at the high-activity period. On the other hand, the shifts are better correlated with the proxies sensitive to changes in the weak component of the magnetic field. Our correlation analysis suggests that more than 90% of the variation in the oscillation frequencies in all activity phases can be explained by changes in both components of the magnetic field. Further, the slopes obtained from the linear regression analysis also differ from phase to phase and show a strong correlation with the correlation coefficients between frequency shifts and solar activity.

Subject headings: Sun: helioseismology – Sun: oscillations – Sun: activity – Sun: magnetic fields

1. Introduction

Understanding the source of the varying solar oscillation eigenfrequencies has been a topic of interest since the mid-eighties. A decrease in low-degree mode frequencies between 1980 (near solar maximum) and 1984 (near solar minimum) was initially reported by Woodard & Noyes (1985). Later, using Big Bear Solar Observatory data, Woodard et al. (1991) showed that the frequencies were strongly correlated with the magnetic field strength. The variation of the frequencies with the changing magnetic activity is now well established. Such changes affect both the central frequencies and the frequency splittings of low-degree (Salabert et al. 2004; Chaplin et al. 2007) as well as intermediate-degree modes (Bachmann & Brown 1993; Jain & Bhatnagar 2003; Antia 2003; Dziembowski & Goode 2005) and exhibit a good correlation between the mode frequencies and the solar activity. The high-degree mode frequencies calculated using the Dynamics Program data of the Michelson Doppler Imager (MDI) on board *Solar and Heliospheric Observatory (SOHO)* also clearly show a solar cycle variation (Rabello-Soares, Korzennik, & Schou 2006).

Detailed studies have shown that the mode frequencies do not always follow the same paths during the rising and the declining phases of the solar activity (Jiménez-Reyes et al. 1998; Tripathy et al. 2001). In addition, using the continuous oscillation data from the Global Oscillation Network Group (GONG) for the rising phase of cycle 23, Howe et al. (1999) demonstrated that, although the average frequency shift is correlated well with measures of surface magnetic activity integrated over the whole disk, the even-order splitting coefficients had a higher correlation with the corresponding coefficients of a Legendre polynomial decomposition of the surface magnetic field than with the total flux. A recent analysis of the year-wise distribution of the frequency shifts with the change in activity indices showed that both the linear-regression slopes and the magnitude of the correlation varied from year to year (Tripathy et al. 2007). Their analysis further demonstrated that there were significant differences between long-term and short-term variations and concluded that averages of short-term variations do not accurately reflect the long-term variations and vice versa. The analysis of Chaplin et al. (2007) for low degree modes involving three solar cycles also indicate that the frequency shifts are primarily sensitive to the weak component of the magnetic flux.

Thus, the relationship between oscillation frequencies and solar activity indicators seems to be more complicated than the linear relation generally demonstrated in earlier studies (Woodard et al. 1991; Bachmann & Brown 1993; Jain & Bhatnagar 2003). With access to the high quality uniform data from GONG and MDI instruments for a nearly complete solar cycle, it is timely to revisit the temporal variability of the frequencies with the progression of solar activity cycle to understand the detailed relationship between them. In this paper,

we closely examine the relationship between the frequency shifts of the intermediate degree modes and nine activity proxies for cycle 23. We further divide the span of the activity cycle into three phases and compare the results obtained for different phases with the entire activity cycle. The frequency and activity data used here are presented in Section 2. We present results for individual data sets and their comparison in Section 3. A possible scenario to explain the variation in oscillation frequencies is discussed in Section 4 and the main findings are summarized in Section 5.

2. Data

2.1. Mode Frequencies

The analysis presented here uses intermediate-degree mode data sets obtained from the GONG¹ and MDI², covering a period of about 12 years i.e. a nearly complete solar cycle starting from 1996 May 1. Each data set consists of centroid frequencies $\nu_{n,\ell}$ and splitting coefficients a_i and each n, ℓ multiplet is represented by a polynomial expansion

$$\nu_{n,\ell,m} = \nu_{n,\ell} + \sum_{i=1}^{i_{max}} a_i(n, \ell) P_i^{(\ell)}(m), \quad (1)$$

where $P_i^{(\ell)}(m)$'s are orthogonal polynomials of degree i and i_{max} is the number of a coefficients used in determining frequencies (Schou 1992). The remaining symbols in equation (1) have their usual meanings. The fitting is done using $i_{max} = 9$ for GONG and 18 for MDI.

For the study reported here, we cover a period from the minimum of solar cycle 23 (1996 May) to the near minimum period of solar cycle 24 (2008 February). The continuous GONG data sets are centered at GONG Month (GM) 12 to 124 while MDI data have two gaps in 1998–99 due to the breakdown of the satellite. It should be also noted that each 108-day GONG data set starts 36 days later than the previous one having an overlap of 72 days while the 72-day MDI data sets are non-overlapping. The MDI data have been obtained from the medium- ℓ program that provides almost continuous coverage to modes with $\ell \leq 300$. Various other details of the data sets are given in Table I and duty cycles are plotted in Figure 1. We further note that the GONG data sets have relatively low duty cycle as compared to the MDI. The number of modes present in each GONG data set varies between 1700–1800, but only one-third of these modes are observed in all 113 overlapping data sets.

¹<ftp://gong.nso.edu/data/>

²<http://quake.stanford.edu/schou/anavw72z/>

Similarly, each MDI data set has approximately 1900 modes, which reduces to 885 common modes in all 58 data sets. The common mode sets in GONG and MDI are shown in Figure 2(a-b). It should be noted that all these common modes are not successfully fitted for both projects, this might be due to the consequence of finite lifetime and stochastic nature of the modes. The common modes observed in both data sets are shown in Figure 2c.

2.2. Proxies for Solar Activity

To study the changes in mode frequencies with solar activity, we have used nine proxies of solar activity probing the solar atmosphere at different heights. Each activity index is briefly summarized below;

1. R_I , the international sunspot number computed from the total number of spots visible on the face of the sun (N) and the number of groups (G) into which they cluster. R_I is equal to $10G + N$.
2. KPVI, the line of sight magnetic field strength observed with 1 arc-sec pixels using the photospheric Fe I line at the Kitt Peak Vacuum Telescope and averaged over the full disk (Livingston et al. 1976).
3. MWSI, the Mt. Wilson sunspot index calculated using Mt. Wilson magnetograms taken at the 150-Foot Solar Tower. MWSI is determined by summing the absolute values of all pixels with a magnetic field strength (> 100 G) which is then divided by the total number of pixels (regardless of magnetic field strength) in the magnetogram (Ulrich 1991).
4. F_{10} , the integrated emission from the solar disc at 2.8 GHz i.e. 10.7 cm wavelength. It mainly represents the contributions from sunspots and radio plagues in the upper chromosphere in addition to the quiet-Sun background emission (Covington 1969; Kundu 1965).
5. He I, the equivalent width of the He I 1083 nm solar absorption line. It is affected by photo-ionization radiation from the upper transition region and corona. The index is calculated by measuring the change in temperature in transition region (Harvey 1984).
6. MPSI, the magnetic plage strength index calculated in the same manner as the MWSI but the absolute value of the magnetic field strength is summed for fields between 10 G and 100 G.

7. Mg II, the Mg II core-to-wing ratio derived by taking the ratio of the h and k lines of the solar Mg II feature at 280 nm to the background or wings at approximately 278 nm and 282 nm. The h and k lines are variable chromospheric emissions while the background emissions are more stable. This ratio is a robust measure of chromospheric activity, mainly for solar UV and EUV emissions (Viereck et al. 2001).
8. TSI, the total solar irradiance, describes the radiant energy emitted by the Sun over all wavelengths that falls each second on 1 square meter outside the earth’s atmosphere. It is affected by the changes in both photospheric and chromospheric magnetic structures. We use observations made by VIRGO instrument on board *SOHO* (Fröhlich et al. 1997).
9. CI, the coronal index measures the total energy emitted by the sun’s outermost atmospheric layer (the corona) at a wavelength of 530.3 nm (Rybansky et al. 1994).

It is worth mentioning that some activity indices are direct measurements of weak, strong or both components of the magnetic field at different heights in the solar atmosphere while others are surrogates of magnetic measurements. The strongest fields are concentrated in flux tubes in sunspots while the larger area around sunspots harbors active regions and their plages contain small-scale pores with relatively weak field strength. The weak components are more widely distributed in latitude than the strong components which are confined to the activity belts. Since flux tubes expand like a canopy in chromosphere above the photospheric footpoints, the field strength decreases with increasing height.

Table 2 summarizes each activity index, including the spectral line of observation, the period of observation used in the analysis, the dominant component of the magnetic field, and the source of the data. A mean activity, I , is computed for each activity index over the same temporal intervals corresponding to the individual frequency measurements. This mean value is used in subsequent calculations.

3. Analysis and Results

3.1. Temporal variation in frequencies

The centroid frequency shift $\delta\nu$ is calculated from the relation

$$\delta\nu(t) = \sum_{n,\ell} \frac{Q_{n,\ell}}{\sigma_{n,\ell}^2} \delta\nu_{n,\ell}(t) / \sum_{n,\ell} \frac{Q_{n,\ell}}{\sigma_{n,\ell}^2}, \quad (2)$$

where $\delta\nu_{n,\ell}(t)$ is the change in the measured frequency with respect to a reference frequency, $\sigma_{n,\ell}$ is the uncertainty in the frequency measurement for a given n, ℓ multiplet and $Q_{n,\ell}$ is the inertia ratio as defined by Christensen-Dalsgaard & Berthomieu (1991). There are several definitions for selecting a reference frequency, which have been discussed in detail by Howe et al. (2002). For a given mode, we adopt an approach of taking a temporal mean over all the available data sets. It has also been shown earlier that the frequency shift is strongly dependent on the frequency and increases with increasing frequency (e.g. see Figure 3 of Jain et al. (2000)). We therefore restrict our analysis to common modes observed in all data sets to obtain an unbiased variation.

We use 235 modes observed in all GONG and MDI data sets in the degree range of $21 \leq \ell \leq 147$, radial order range of $1 \leq n \leq 16$ and the frequency range of $1.5 \leq \nu \leq 4.0$ mHz. These modes are shown in Figure 2c. The reference frequencies are calculated by taking an average of the frequencies of a particular multiplet (n, ℓ) from all of the available GONG and MDI data sets. Figure 3 shows the temporal variation of frequency shift for both data sets. The dashed line depicts the variation of the solar activity represented by radio flux, F_{10} . It is clearly seen that the frequencies vary in phase with the solar activity as shown in earlier studies (e.g. Jain & Bhatnagar (2003); Chaplin et al. (2007)). We also note that there is a systematic offset between GONG and MDI frequency shifts, which is consistent with the findings of Howe et al. (2002). The MDI frequency shifts are consistently higher than the GONG and this deviation is relatively large at the low activity periods. However, the overall shifts from the minimum to the maximum in both cases are approximately same. The discrepancy observed might be due to the fact that the GONG and the MDI pipelines consider time series of different lengths and use different mathematical methods to determine the mode frequencies. A detailed correlation analysis between the frequency shifts and solar activity is presented in the next section.

3.2. Correlation with solar activity

3.2.1. Solar cycle variation

The temporal variations in frequency shifts with various measures of the solar activity are plotted in Figures 4 and 5 for GONG and MDI data sets, respectively. Although the frequency shifts follow the general trend of the solar activity, there are variations between different activity indices. For example, we note discrepancies between $\delta\nu$, and R_1 , MWSI and TSI at high activity period. We examine this variation by calculating the correlation between them. This is displayed in Table 3, where linear (r_P) and rank (r_S) correlation coefficients between frequency shifts and the measures of solar activity are tabulated. The

linear correlation coefficient is an estimate of the linear relationship between the two sets and the rank correlation shows whether one set of numbers has any effect on another set of numbers. The high values of r_P (≥ 0.9) clearly indicate a linear relationship between two quantities. Therefore, we fit the shifts against activity using linear expression

$$\delta\nu = a + bI \tag{3}$$

and investigate the sensitivity of frequency shifts on solar activity. The slope, b , which measures the shift per activity index, and intercept, a , obtained from the linear least-square fit for each activity index, I , are also given in Table 3. The gradients obtained from the linear regression analysis show a higher sensitivity in the GONG data as compared to the MDI and is consistent with the notion that the uncertainty in the determination of frequencies is inversely proportional to the square root of the length of the time series.

A comparison of correlation coefficients for all activity indices indicates that the best correlation is obtained for chromospheric activity indices, in particular F_{10} . The recent analysis of low-degree modes also report better correlations for F_{10} , He I equivalent width and Mg II core-to-wing ratio for three consecutive cycles 21–23 (Chaplin et al. 2007). However, these authors report relatively low correlation coefficients for these indices as compared to our analysis, although the length of the time samples in both cases is the same, i.e. 108 days. The low-degree modes travel deep to the solar interior while the intermediate degree modes are confined to the radiation and convection zones. Virtually all of the activity effects on the modes is at the surface. The surface spatial patterns of the low- ℓ modes are not well matched to the spatial distribution of surface activity, hence one may expect intermediate- and high-degree modes to correlate better with the activity. We also obtain higher correlation coefficients for the 108-day GONG data sets compared to the 72-day MDI data. The analysis of Chaplin et al. (2001) and Tripathy et al. (2007) on many different time scales show similar correlation patterns.

Although cycle 23 has been a weak cycle compared to its predecessor, it recorded two prominent peaks during solar maximum. The first peak in sunspot number (mid-2000) was higher than the secondary peak (late-2001), while several other solar indices (e.g., KPML, F_{10} , Mg II) had a maximum at the secondary peak. The frequency shifts also exhibited the maximum during the secondary peak. Thus R_I is the only activity proxy whose maximum does not coincide with the maximum of the frequency shifts.

3.2.2. Phase-wise variation

In order to study the correlation between frequency shifts and activity at different phases of the solar cycle, we divide the activity cycle into three phases; the rising activity period from 1996 September 22 to 1999 June 26 (*Phase I*), the high-activity period from 1999 June 27 to 2003 January 12 (*Phase II*), and the declining activity period from 2003 January 13 to 2007 July 26 (*Phase III*). It should be noted that the relatively flat portion of solar activity corresponding to the beginning of minimum phase is not included in this analysis. The start and end dates in each activity phase are the same for both GONG and MDI data sets. The number of data sets representing *Phase I, II and III* are; 26 (GM 16 - 41), 34 (GM 44 - 77) and 44 (GM 80 - 123) for GONG and 11, 17 and 22 for MDI. Our analysis is restricted to *Phases I and II* for indices KPMI and He I due to the unavailability of activity data during the entire declining phase.

The calculated linear correlation coefficients, r_P , for both GONG and MDI data sets for all the three phases are shown in Figure 6. In the same figure, we also compare these coefficients with those obtained for the complete cycle. It is interesting to note that the correlation between frequency shifts and solar activity changes significantly from phase to phase except for F_{10} . In all cases, the rising and the declining phases are better correlated than the high-activity phase, except for CI where we obtain a decrease in correlation during the declining phase for the frequency shifts calculated from GONG. A substantial decrease in correlation during high-activity phase is obtained for R_1 , MWSI, TSI and He I indices. This poor correlation is also visible in Figures 4 and 5 where variation in $\delta\nu$ shows a different pattern than the activity proxies. We point out that the R_1 , MWSI and TSI indices are most affected by the sunspots with strong magnetic fields, while other proxies (e.g. MPSI, Mg II) are sensitive to the weak component of the magnetic field (see Table 2). The KPMI and F_{10} indices are modulated by both components, however the dominant contribution to F_{10} comes from the weak component. The change in correlation coefficients for He I is similar to that we obtain for CI, but the coefficients for the declining phase can not be compared due to insufficient measurements of the He I index. It should be noted here that these two indices are influenced by the changes occurring above the chromosphere.

Because the correlation coefficients clearly reveal a phase-wise variation, we further investigate their relation to the corresponding linear regression slopes. The slopes for different phases calculated using Equation 3 are tabulated in Table 4. It is seen that the slopes in the rising and falling phases are greater than that obtained for the high activity period. However, KPMI appears to be an exceptional case where the slopes in the high activity period are marginally higher (within 1σ error) than the rising activity period, for both GONG and MDI data sets.

The calculated linear correlation coefficients between phase-wise correlation coefficients and slopes ($r_P([r_P(I, \delta\nu)], [b])$), and solar activity ($r_P([r_P(I, \delta\nu)], [I])$) for different activity indicators are summarized in Table 5 for both GONG and MDI data sets. In all cases, except for CI, we obtain a significant positive correlation between correlation coefficients and slopes, and a negative correlation between correlation coefficients and activity indices. In general, we find that the GONG data has a higher correlation than the MDI data. Our results are further consistent with the findings of Tripathy et al. (2007) where year-wise variations in the linear-regression slopes and the correlation coefficients are measured from frequencies that were determined from time series of 9 days. They also found a positive correlation between these two but no significant correlation or anti-correlation between the slopes and the solar activity. This difference may be attributed to the fact that the frequency shifts track the changes in solar activity much better on longer time scales, as discussed in the previous subsection.

3.3. Comparison between rising and declining phases: the hysteresis patterns

As shown in Section 3.2.2, there is no significant difference between correlation coefficients in rising and declining phases, except for CI, one may expect that the curves of frequency shifts plotted against solar activity during the two separate phases should overlap with each other or have a constant shift between them. However, the magnetic field indices in cycle 22 have been found to follow different curves during ascending and descending phases, exhibiting a hysteresis loop (Jiménez-Reyes et al. 1998; Tripathy et al. 2001). It is also shown that not all activity indices have a linear relationship among them (Bachmann & White 1994). Since cycle 23 has been referred to as *anomalous* solar cycle (de Toma et al. 2004) due to differences in various activity measures as compared to other cycles, we plot frequency shifts against the activity and examine the behavior of these curves to obtain a deeper insight of the variation of frequencies with solar activity.

In Figures 7 and 8, we show the variation of $\delta\nu$ as a function of four different activity indices (F_{10} , KPMI, MPSI and Mg II) for GONG and MDI data sets, respectively. The open and filled symbols represent the ascending and descending phase, respectively; the high activity period is shown by *asterisk* symbols. It is evident that the mode frequency shifts follow similar paths during the ascending and descending phases for the radio flux, F_{10} , and full-disk magnetic field, KPMI. However, the other two pairs (MPSI, and Mg II) exhibit different paths and form a broader curve. The behavior of F_{10} , MPSI and Mg II in cycle 23 is consistent with that for cycle 22 while the variation of frequencies with KPMI contradicts the findings of Jiménez-Reyes et al. (1998) and Tripathy et al. (2001). We note

that the instrument at Kitt Peak was upgraded in 1992 to reduce the noise level. The post-upgrade data were calibrated to place them at the same scale as pre-upgrade data but any systematic offset between the two data sets could lead to a constant shift in the values of KPMI and may account for the hysteresis pattern seen in cycle 22.

4. Discussion

The intermediate-degree modes are generally confined to the convection zone, therefore one may expect the variation in their characteristics to be influenced by changes in this region. The solar cycle related shifts are believed to occur primarily at the surface reflection of the modes. In addition, their variation and strong correlation with solar activity indices over the solar cycle provide sufficient evidence for their association with the changing solar magnetic activity. Various measurements have been made to estimate such changes in magnetic activity. In this analysis, we have considered three proxies which represent quantitative measurements of the magnetic field strength, i.e. KPMI, MWSI and MPSI. As outlined earlier, the KPMI is total line-of-sight magnetic field while MWSI provides only the strong component in the photosphere. On the other hand, MPSI estimates weak fields associated with magnetic plages in the chromosphere.

In order to study the differences in the correlation between frequency shifts and various magnetic measurements, we plot 108-day averaged photospheric fields against the MPSI (Figure 9). Note that the weak and strong fields do not vary in a similar way at all activity phases. We find a linear relationship during rising and falling activity periods among all three proxies, but a large deviation from the linear trend is seen between MPSI and MWSI during the high-activity period. The variation in the KPMI is linear with the MPSI in rising- and high-activity periods, however, their behavior remains unexplored during the declining phase due to the unavailability of KPMI data. To supplement the KPMI measurements during the declining phase, we include in the same figure the line-of sight magnetic field measured by Synoptic Optical Long-term Investigations of the Sun (SOLIS) instrument located at Kitt Peak. The SOLIS observations³ are made using a different spectral line (Fe I 630.2 nm) than the KPMI, but the overlapping data of these two instruments show a similar response to active regions and other solar phenomena (J. W. Harvey, private communication). However, we notice a downward shift in the SOLIS fields as compared to the KPMI which may be due to the use of a different spectral line. Moreover, we find a strong correlation between SOLIS magnetic field and the MWSI which is consistent with the results obtained for KPMI.

³http://solis.nso.edu/vsm/svsm_m11_meanfield.dat

Therefore, we do not expect frequency shifts to correlate equally with all activity indicators at different phases. Our analysis for the complete cycle and different activity phases clearly shows that the frequency shifts have the best correlation with the 10.7 cm radio flux. The radio flux is measured in the high chromosphere and lower corona, but it is modified by the evolution of sunspots (strong magnetic field) and radio plages (weak magnetic field). By analyzing low- ℓ frequencies for cycle 21–23, Chaplin et al. (2007) concluded that the frequencies have good sensitivity to the effects of the weak component of the magnetic fields. Recently, Tripathy et al. (2007) have shown that activity related changes in oscillation frequencies can be tracked on a time scale as short as nine days. They also obtained the best correlation with the radio flux. In a theoretical study, Campbell & Roberts (1989) also showed that changes in the chromospheric magnetic field strength can cause changes in the p -mode frequencies at higher ℓ (≥ 100). On the other hand, using the technique of local helioseismology, Hindman et al. (2000) argued that the magnitude of the variation in frequencies depend upon the magnetic field strength associated with active regions on the solar surface and the physical phenomenon inducing the shifts is confined to the surface layers of the Sun. On the basis of our study, we find that both components of the magnetic field influence the changes in the oscillation frequencies, however the weak component plays a dominant role. To examine this conclusion, we developed various regression models between MWSI (strong magnetic field), MPSI (weak magnetic field), and F_{10} and $\delta\nu$ from GONG and MDI data sets. The variance for different regression models calculated using frequency shifts from GONG data are given Table 6. It is clearly seen that we obtain higher correlation at all activity phases for the models based on either F_{10} or combined MPSI and MWSI data. These models are able to explain more than 90% of the variation in the frequencies at all activity phases. In contrast, the model with strong component of magnetic field (MWSI) explains less than 50% of the variation while the model with only weak component (MPSI) explains less than 80% of the variation in frequencies at high-activity period. A similar behavior is also seen in case of MDI data.

5. Summary

The improved and continuous measurements of intermediate-degree p -mode frequencies for a complete solar cycle demonstrate that, while the frequencies vary in phase with the solar activity, the degree of correlation between the frequency shifts and activity indices differs from one phase of activity to another.

Although there is a strong correlation between frequency shifts and all activity proxies during the rising and declining phases, we find a significant change in the correlation at

the high-activity period. The maximum decrease is obtained for R_I , MWSI, TSI, and He I, where first three indices are most affected by the sunspots with strong magnetic fields in the photosphere while He I is influenced by the change in temperature in transition region. The change in correlation coefficients for CI is similar to that of He I but we could not compare the coefficients in the declining phase due to insufficient measurements of the He I index. We further find a negligible change in the correlation for the 10.7 cm radio flux which provides estimates of the variation in both weak and strong components of the magnetic field. It is also influenced by a slowly varying component (S -component) that originates thermally in localized regions of high electron densities and magnetic fields present in the vicinity of sunspot and chromospheric plages. These regions remain present over several rotations of the Sun and contribute to the change in oscillation frequencies. Our analysis suggests that both components of the magnetic field contribute significantly to the variation in oscillation frequencies, however the contribution from the weak component appears to be dominant.

The correlation coefficients are strongly correlated with the slopes obtained from the linear regression analysis, in agreement with the earlier findings of Tripathy et al. (2007) using frequencies determined from time-series of 9 days in length. In addition, slopes and correlation coefficients are found to be strongly anti-correlated with the measures of solar activity. However, the coronal index shows a poor correlation in all cases. It may be due to the fact that the solar oscillations are most affected by the magnetic activity of lower atmosphere and are not influenced by the changes in corona.

We thank the anonymous referee for useful comments. We also thank Mukul Kundu and Bill Livingston for useful discussions. This work utilizes data obtained by the Global Oscillation Network Group (GONG) project, managed by the National Solar Observatory, which is operated by AURA, Inc. under a cooperative agreement with the National Science Foundation. The data were acquired by instruments operated by the Big Bear Solar Observatory, High Altitude Observatory, Learmonth Solar Observatory, Udaipur Solar Observatory, Instituto de Astrofísica de Canarias, and Cerro Tololo Interamerican Observatory. It also utilizes data from the Solar Oscillations Investigation/Michelson Doppler Imager on the Solar and Heliospheric Observatory. SOHO is a mission of international cooperation between ESA and NASA. NSO/Kitt Peak magnetic, and Helium measurements used here are produced cooperatively by NSF/NOAO; NASA/GSFC and NOAA/SEL. SOLIS data used here are produced cooperatively by NSF/NSO and NASA/LWS. This study also includes data from the synoptic program at the 150-Foot Solar Tower of the Mt. Wilson Observatory. The Mt. Wilson 150-Foot Solar Tower is operated by UCLA, with funding from NASA, ONR and NSF, under agreement with the Mt. Wilson Institute. The unpublished solar irradiance data set (version v6_001_0804) was obtained from VIRGO Team through PMOD/WRC, Davos,

Switzerland. This work has made use of NASA's Astronomy data System (ADS) and data available at NOAA's National Geophysical Data Center (NGDC) website. This work was supported by NASA grant NNG 05HL41I and NNG 08EI54I.

REFERENCES

- Antia, H. M. 2003, *ApJ*, 590, 567
- Bachmann, K. T., & Brown, T. M. 1993, *ApJ*, 411, L45
- Bachmann, K. T., & White, O. R. 1994, *Sol. Phys.*, 150, 347
- Campbell, W. R., & Roberts, B. 1989, *ApJ*, 338, 538
- Chaplin, W. J., Elsworth, Y., Isaak, G. R., Marchenkov, K. I., Miller, B. A., & New, R. 2001, *MNRAS*, 322, 22
- Chaplin, W. J., Elsworth, Y., Miller, B. A., & Verner, G. A. 2007, *ApJ*, 659, 1760
- Christensen-Dalsgaard, J., & Berthomieu, J. 1991, in *Solar Interior and Atmosphere*, eds. A. N. Cox, W. C. Livingston, M. Matthews (Tucson: University of Arizona Press), 401
- Covington, A. E. 1969, *JRASC*, 63, 125
- de Toma, G., White, O. R., Chapman, G. A., Walton, S. R., Preminger, D. G., & Cookson, A. M. 2004, *ApJ*, 609, 1140
- Dziembowski, W. A., & Goode, P. R. 2005, *ApJ*, 625, 548
- Fröhlich, C., Crommelynck, D., Wehrli, C., Anklin, M., Dewitte, S., Fichot, A., Finsterle, W., Jiménez, A., Chevalier, A., & Roth, H. J. 1997, *Sol. Phys.*, 175, 267
- Harvey, J. W. 1984, NASA, Washington Solar Irradiance Variations on Active Region Time Scales (SEE N84-27635 17-92), 197
- Hindman, B., Haber, D., Toomre, J., & Bogart, R. S. 2000, *Sol. Phys.*, 192, 363
- Howe, R., Komm, R., & Hill, F. 1999, *ApJ*, 524, 1084
- Howe, R., Komm, R., & Hill, F. 2002, *ApJ*, 580, 1172
- Jain, K., & Bhatnagar, A. 2003, *Sol. Phys.*, 213, 257
- Jain, K., Tripathy, S. C., & Bhatnagar, A. 2000, *ApJ*, 542, 521

- Jiménez-Reyes, S. J., Régule, C., Palle, P. L., & Roca Cortés, T. 1998, *A&A*, 329, 1119
- Kundu, M. R. 1965, *Solar Radio Astronomy* (New York: Interscience Publication)
- Livingston, W. C., Harvey, J., Slaughter, C., & Trumbo, D. 1976, *Appl. Opt.*, 15, 40
- Rabello-Soares, M. C., Korzennik, S. G., & Schou, J. 2006, in *ESA SP-624, Proceedings of SOHO18/GONG 2006/HELAS I, Beyond the Spherical Sun*, eds. K. Fletcher & M. J. Thompson (Noordwijk: ESA), 71
- Rybansky, M., Rusin, V., Minarovjech, M., & Gaspar, P. 1994, *Sol. Phys.*, 152, 153
- Salabert, D., Fossat, E., Gelly, B., Kholikov, S., Grec, G., Lazrek, M., & Schmider, F. X. 2004, *A&A*, 413, 1135
- Schou, J. 1992, Ph.D. Thesis, Aarhus University, Aarhus, Denmark.
- Tripathy, S. C., Kumar, B., Jain, K., & Bhatnagar, A. 2001, *Sol. Phys.*, 200, 3
- Tripathy, S. C., Hill, F., Jain, K., & Leibacher, J. W. 2007, *Sol. Phys.*, 243, 105
- Ulrich, R. K. 1991, *Adv. Space Res.*, 11, 217
- Viereck, R., Puga, L., McMullin, D., Judge, D., Weber, M., & Tobiska, W. K. 2001, *Geophys. Res. Lett.*, 28, 1343
- Woodard, M. F., & Noyes, R. W. 1985, *Nature*, 318, 449
- Woodard, M. F., Libbretch, K. G., Kuhn, J., & Murray, N. 1991, *ApJ*, 373, L81

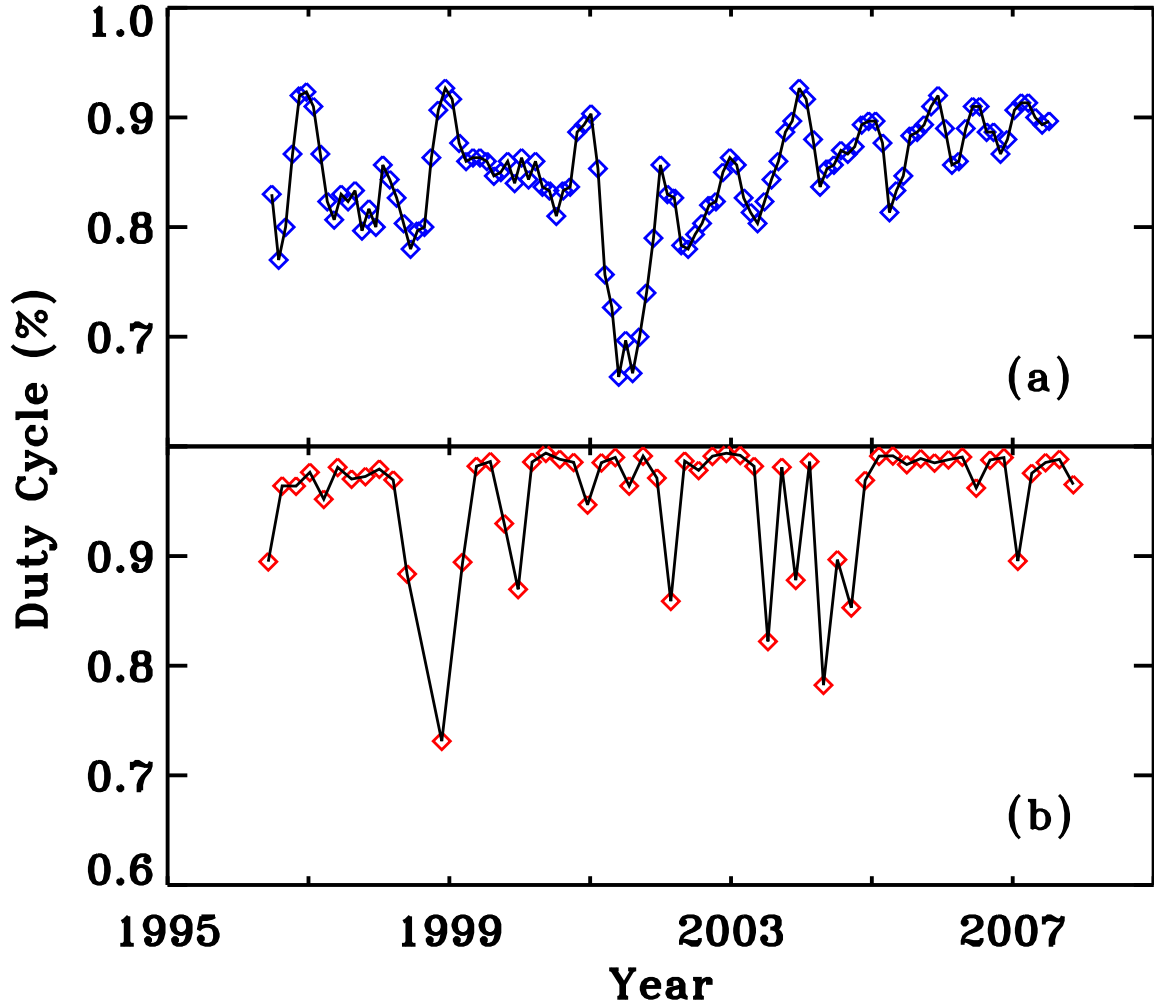


Fig. 1.— Duty cycles of (a) GONG and (b) MDI time series.

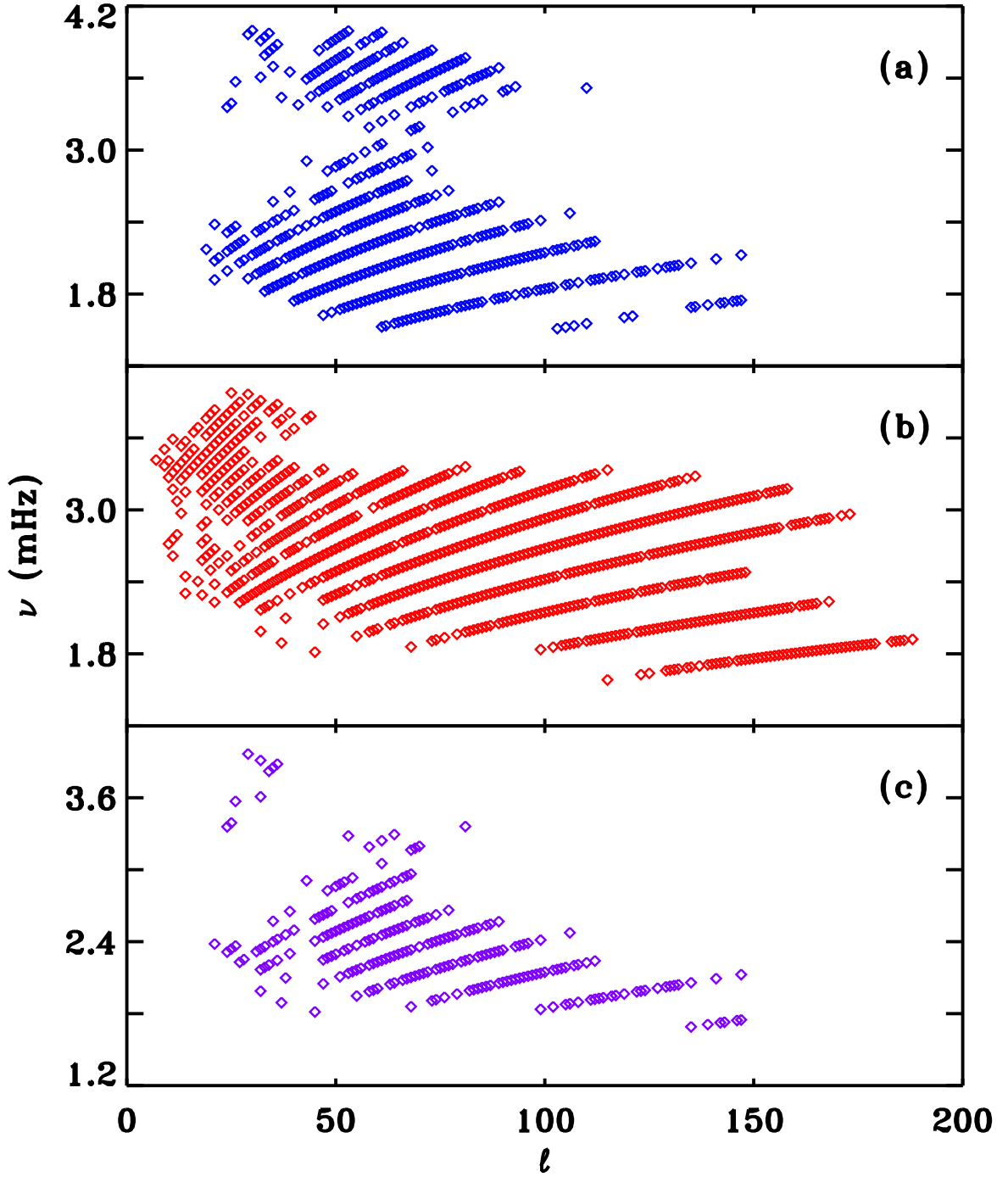


Fig. 2.— Comparison of common p modes observed in all (a) GONG, (b) MDI and (c) combined GONG and MDI data sets.

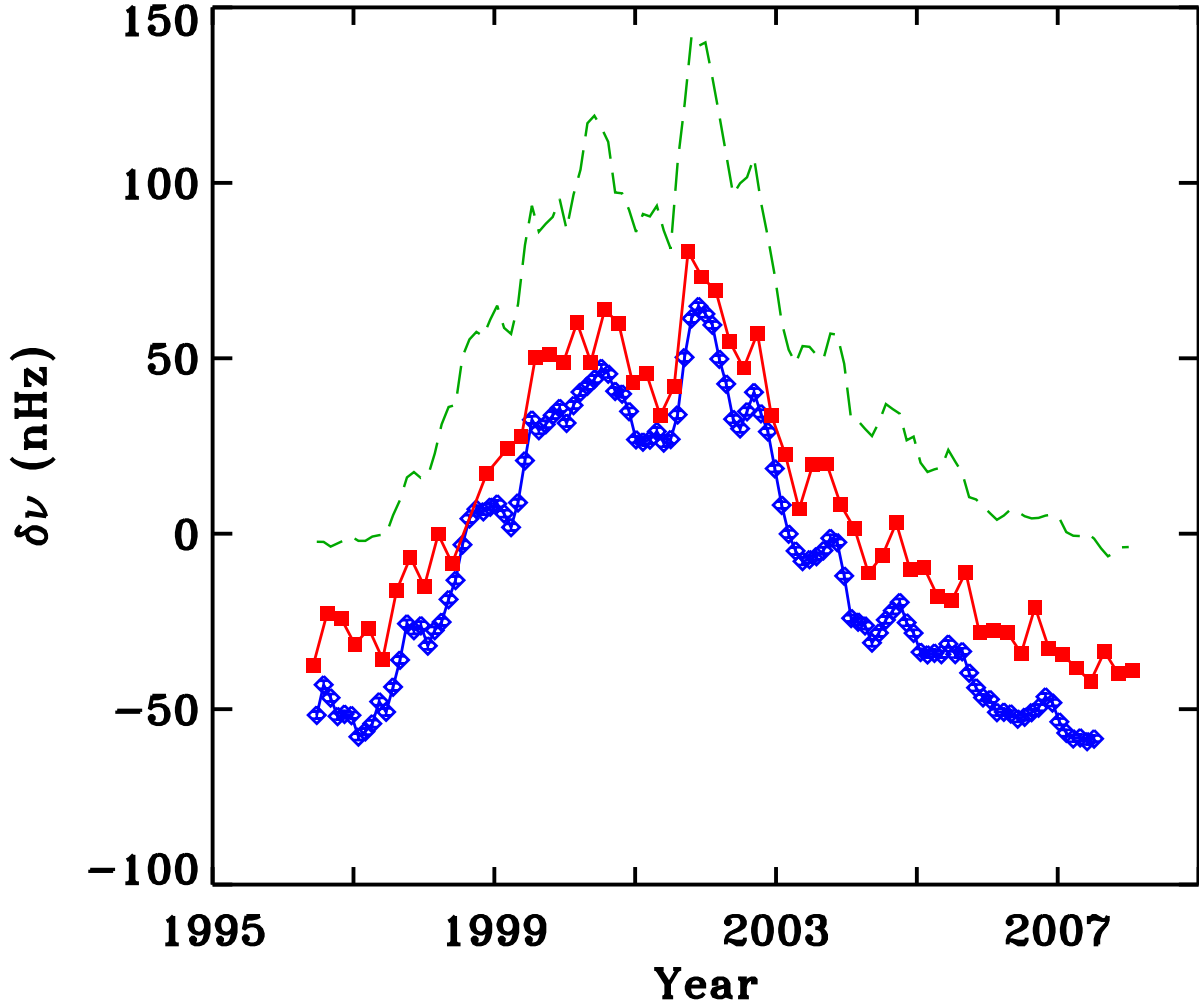


Fig. 3.— Temporal evolution of frequency shifts calculated from the GONG (open symbols) and MDI (filled symbols) frequencies. The dashed line represents the scaled 10.7 cm radio flux.

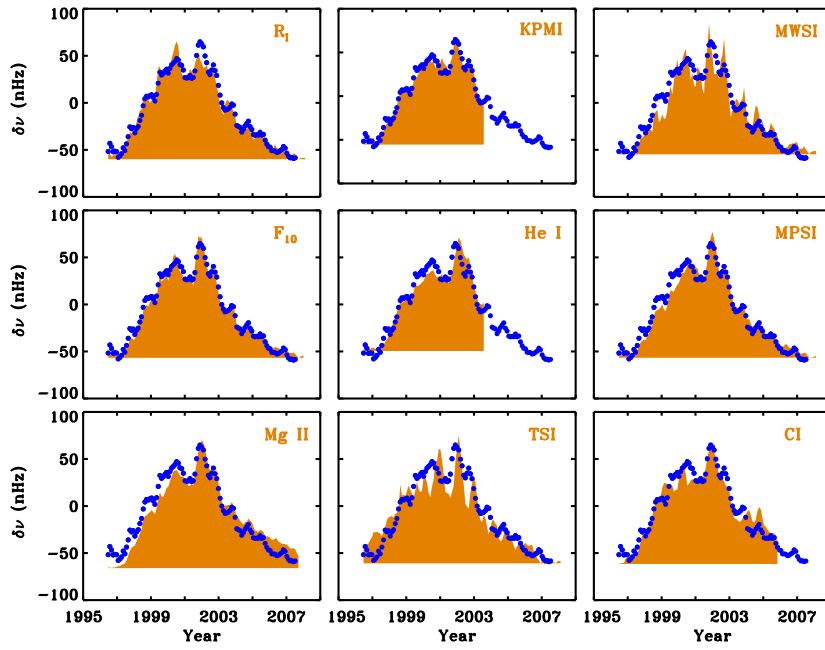


Fig. 4.— Temporal evolution of the GONG frequency shifts (symbols) with different activity proxies (filled regions).

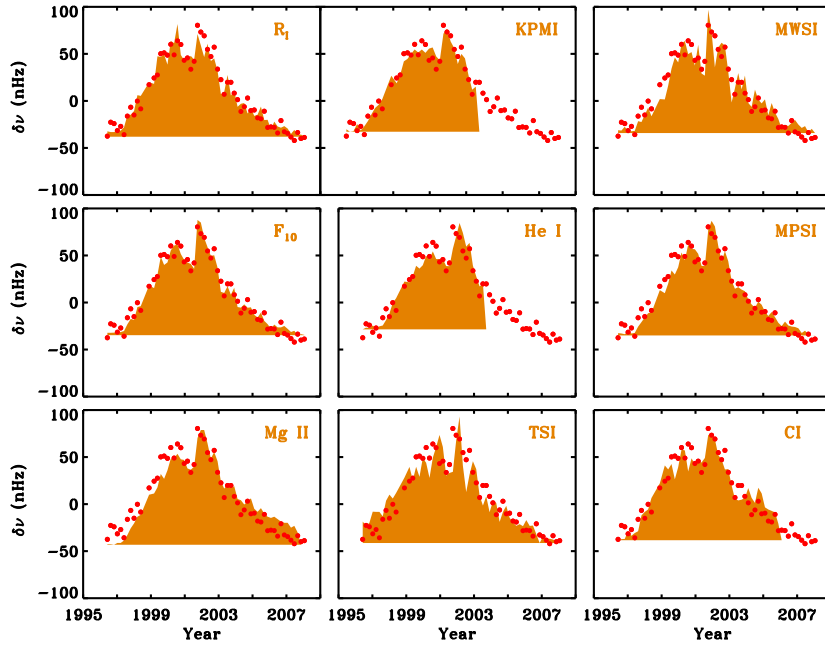


Fig. 5.— Same as Figure 4 but for the shifts calculated from the MDI frequencies.

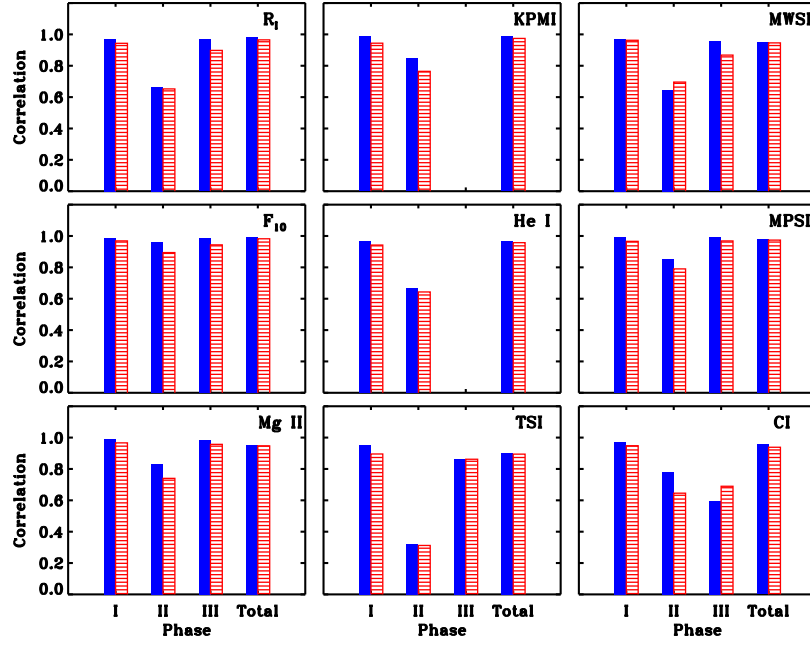


Fig. 6.— Bar-chart showing phase-wise variation of the Pearson’s linear correlation coefficients for different activity indices. The complete solar cycle is divided into three phases; the rising (I), high (II) and declining (III) activity. Each activity phase has values for the GONG (left) and the MDI (right). Note that missing values for KPMI and He I are due to unavailability of activity measurements during the declining phase.

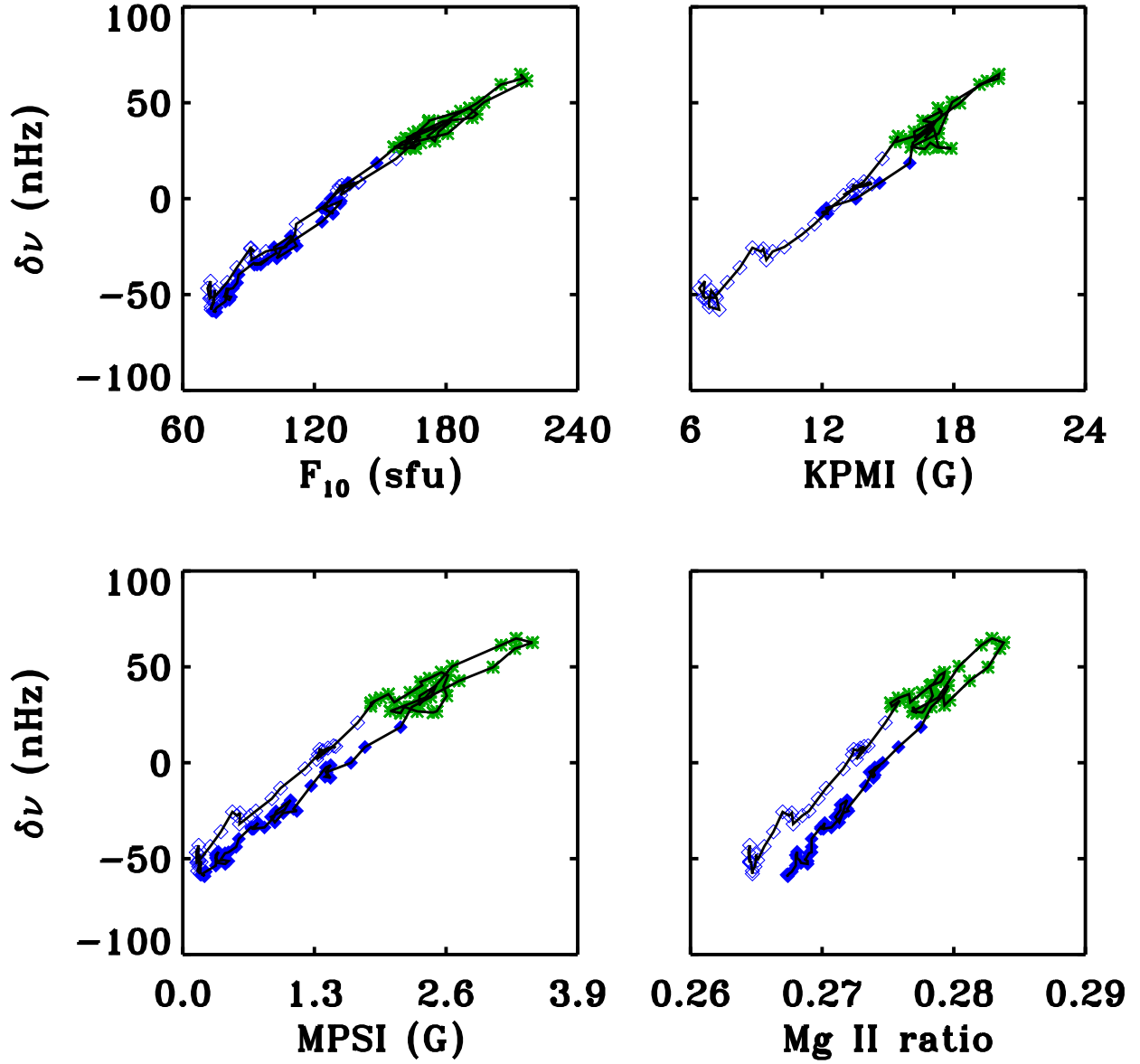


Fig. 7.— Variation of GONG frequency shifts with different activity proxies. The rising, high and falling phases are shown by open symbols, asterisks and filled symbols, respectively. The symbols have been joined by solid line to guide the eye.

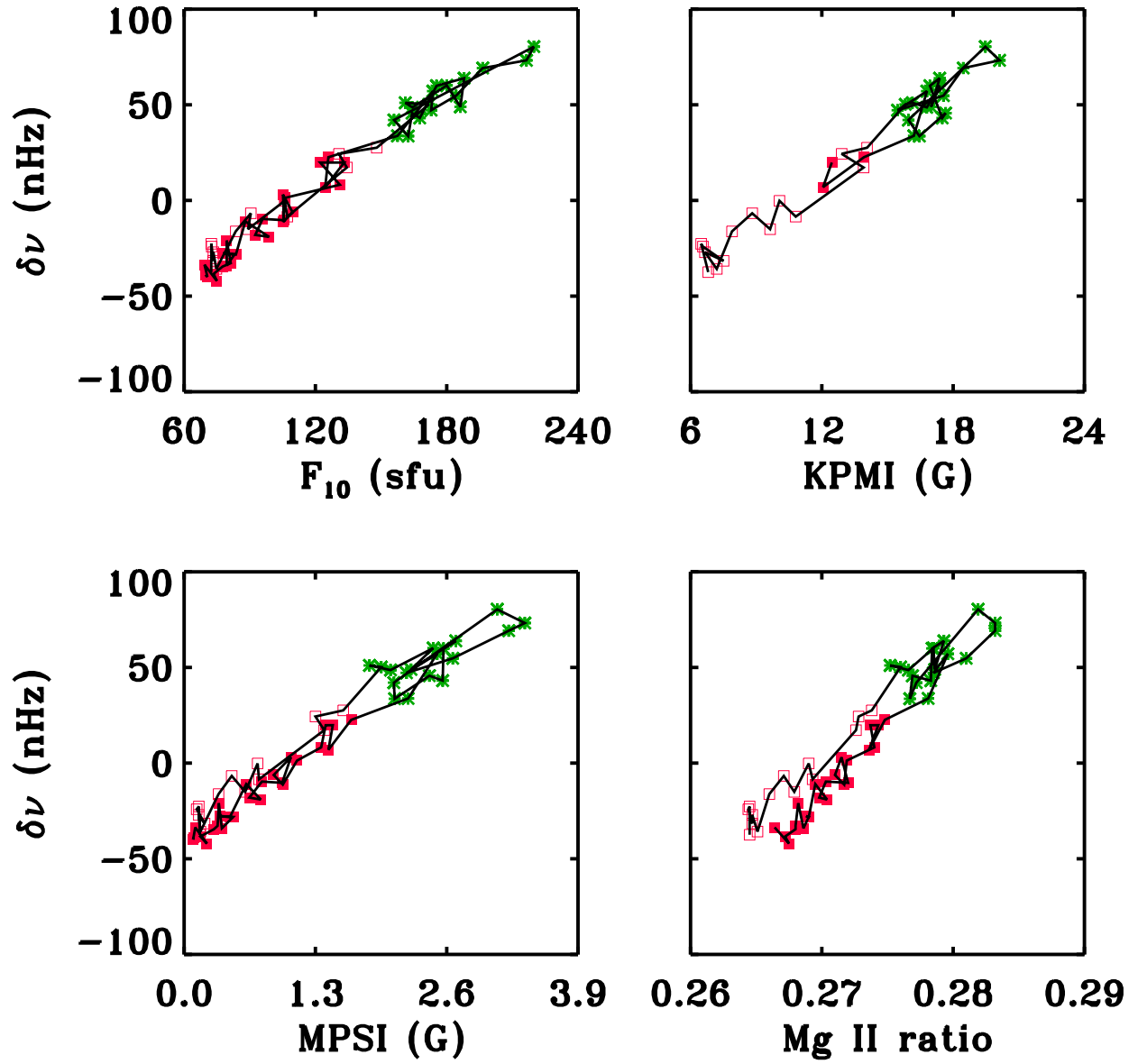


Fig. 8.— Same as Figure 7 but for the MDI frequency shifts.

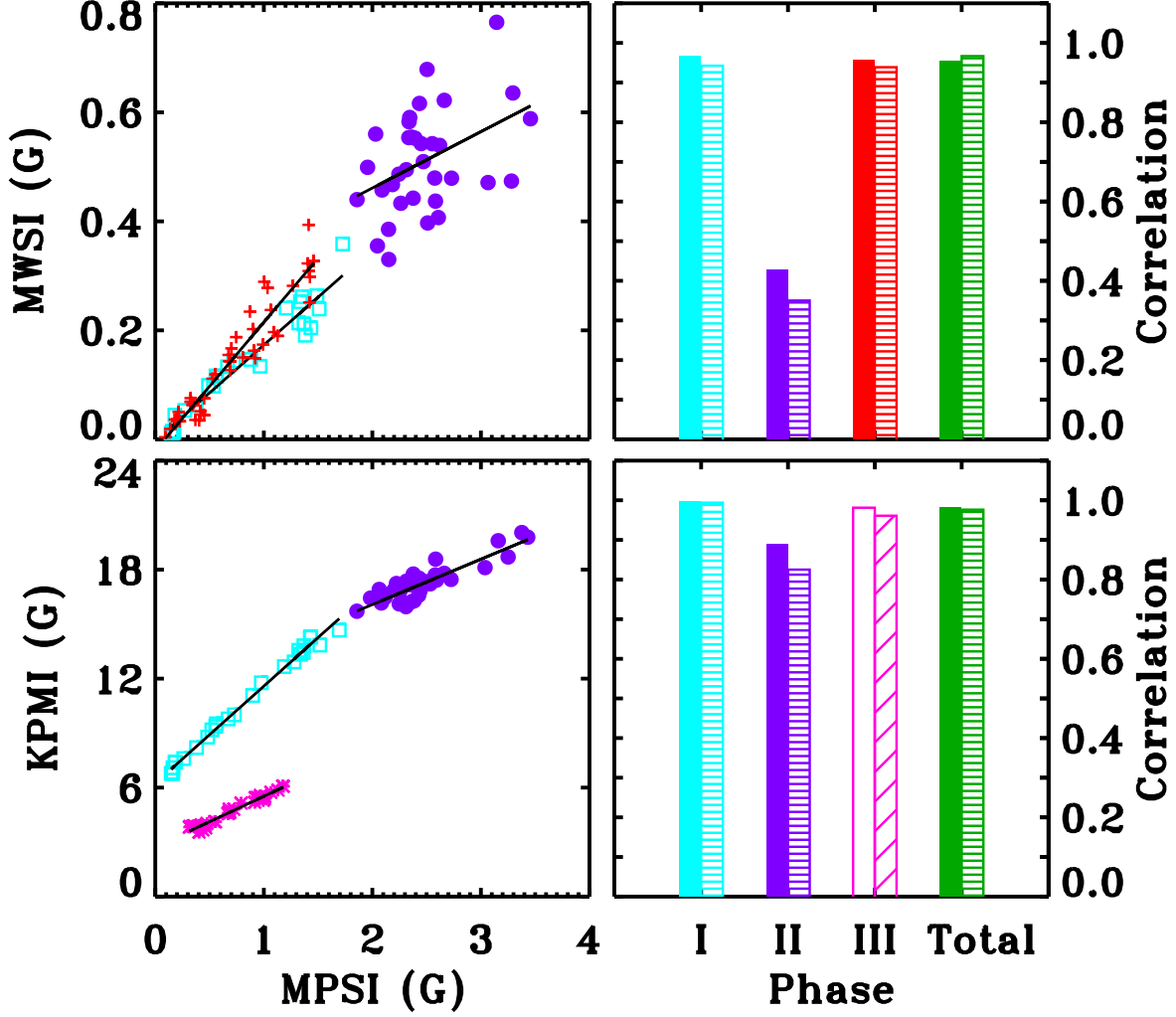


Fig. 9.— (*left*) Variation in KPMI (total field) and MWSI (strong field) as a function of MPSI (weak field). Rising, high and falling activity periods are shown by the squares, filled circles and pluses, respectively. The crosses are for the SOLIS data. The solid lines denote the linear fits at different phases. (*right*) The linear correlation coefficients, r_P (filled) and rank correlation coefficients, r_S (hatched) at different phases corresponding to the left panels. In the lower panel, r_P and r_S between the SOLIS measurements and MPSI are shown by open and diagonally hatched bars, respectively.

Table 1. Description of frequency data sets.

	GONG	MDI
Period	1996 May 1 - 2007 Aug 31	1996 May 1 - 2008 Feb 27
Number of datasets	113	58
Extent (days)	108	72
Frequency range (mHz)	$1.5 \leq \nu \leq 4.0$	$1.5 \leq \nu \leq 4.0$
Number of common modes	500	885
Degree range	$19 \leq \ell \leq 147$	$7 \leq \ell \leq 188$
Radial nodes	$1 \leq n \leq 19$	$1 \leq n \leq 21$

Table 2. Various proxies for solar activity.

Activity Index	Spectral line	Influential field component	End date ^a	Data source
R _I	-	Strong	2008 27 Feb	ftp://ftp.ngdc.noaa.gov/STP/SOLAR_DATA/SUNSPOT_NUMBERS/
KPMI	Fe I 868.8 nm	Both	2003 Sep 21	ftp://nsokp.nso.edu/kpvt/daily/stats/mag.dat
MWSI	Fe I 525.0 nm	Strong	2008 27 Feb	ftp://howard.astro.ucla.edu/pub/obs/mpsi_data/index.dat
F ₁₀	-	Both	2008 Feb 27	ftp://ftp.ngdc.noaa.gov/STP/SOLAR_DATA/SOLAR_RADIO/FLUX/
He I	He I 1083.0 nm	-	2003 Sep 21	ftp://nsokp.nso.edu/kpvt/daily/stats/he.dat
MPSI	Na I 589.5 nm	Weak	2008 27 Feb	ftp://howard.astro.ucla.edu/pub/obs/mpsi_data/index.dat
Mg II	Mg II 279.9 nm	Weak	2007 Oct 6	http://www.sec.noaa.gov/ftplib/sbuiv/NOAAMgII.dat
TSI	-	-	2008 Feb 27	ftp://ftp.pmodwrc.ch/pub/data/irradiance/virgo/TSI
CI	Fe XIV 530.3 nm	-	2005 Dec 31	ftp://ftp.ngdc.noaa.gov/STP/SOLAR_DATA/SOLAR_CORONA/

^aStart date for all data sets is 1996 May 1.

Table 3. The correlation coefficients and the linear regression parameters between activity indices (I) and frequency shift ($\delta\nu$) for the total period covered in this analysis. Shown here are the Pearson’s linear coefficient (r_P), Spearman’s rank correlation (r_S), the intercept (a) and the mean shift per unit change in activity (b). The two-sided significance (P_S) is smaller than 10^{-16} and is not shown here.

Activity Index	Data Source	$r_P(I, \delta\nu)$	$r_S(I, \delta\nu)$	a (μHz)	b (μHz per activity unit)
R_I	GONG	0.98	0.98	$-6.28 \times 10^{-2} \pm 1.60 \times 10^{-4}$	$9.07 \times 10^{-4} \pm 2.28 \times 10^{-6}$
	MDI	0.97	0.95	$-4.01 \times 10^{-2} \pm 2.25 \times 10^{-4}$	$8.31 \times 10^{-4} \pm 3.22 \times 10^{-6}$
KPMI	GONG	0.99	0.96	$-1.11 \times 10^{-2} \pm 4.09 \times 10^{-4}$	$8.63 \times 10^{-3} \pm 2.87 \times 10^{-5}$
	MDI	0.98	0.93	$-8.47 \times 10^{-2} \pm 5.92 \times 10^{-4}$	$8.02 \times 10^{-3} \pm 4.16 \times 10^{-5}$
MWSI	GONG	0.95	0.95	$-5.54 \times 10^{-2} \pm 1.48 \times 10^{-4}$	$1.83 \times 10^{-1} \pm 4.75 \times 10^{-4}$
	MDI	0.95	0.94	$-3.43 \times 10^{-2} \pm 2.10 \times 10^{-4}$	$1.67 \times 10^{-1} \pm 6.59 \times 10^{-4}$
F_{10}	GONG	0.99	0.98	$-1.17 \times 10^{-1} \pm 2.80 \times 10^{-4}$	$8.76 \times 10^{-4} \pm 2.18 \times 10^{-6}$
	MDI	0.98	0.97	$-9.11 \times 10^{-2} \pm 3.95 \times 10^{-4}$	$8.14 \times 10^{-4} \pm 3.10 \times 10^{-6}$
He I	GONG	0.97	0.95	$-1.84 \times 10^{-1} \pm 6.59 \times 10^{-4}$	$2.89 \times 10^{-3} \pm 9.81 \times 10^{-6}$
	MDI	0.96	0.95	$-1.55 \times 10^{-1} \pm 9.58 \times 10^{-4}$	$2.71 \times 10^{-3} \pm 1.42 \times 10^{-5}$
MPSI	GONG	0.98	0.97	$-5.98 \times 10^{-2} \pm 1.54 \times 10^{-4}$	$3.97 \times 10^{-2} \pm 1.00 \times 10^{-4}$
	MDI	0.98	0.97	$-3.83 \times 10^{-2} \pm 2.19 \times 10^{-4}$	$3.71 \times 10^{-2} \pm 1.43 \times 10^{-4}$
Mg II	GONG	0.95	0.94	$-1.92 \pm 4.96 \times 10^{-3}$	$7.01 \pm 1.82 \times 10^{-2}$
	MDI	0.95	0.93	$-1.75 \pm 7.22 \times 10^{-3}$	$6.49 \pm 2.65 \times 10^{-2}$
TSI	GONG	0.91	0.89	$-108.83 \pm 2.95 \times 10^{-1}$	$7.97 \times 10^{-2} \pm 2.16 \times 10^{-4}$
	MDI	0.91	0.90	$-104.31 \pm 4.32 \times 10^{-1}$	$7.64 \times 10^{-2} \pm 3.16 \times 10^{-4}$
CI	GONG	0.96	0.94	$-8.37 \times 10^{-2} \pm 2.69 \times 10^{-4}$	$1.18 \times 10^{-2} \pm 3.59 \times 10^{-5}$
	MDI	0.94	0.92	$-5.84 \times 10^{-2} \pm 3.88 \times 10^{-4}$	$1.08 \times 10^{-2} \pm 5.17 \times 10^{-5}$

Table 4. Calculated linear regression slopes (in μHz per activity unit) for different activity phases of solar cycle. Note that the slopes for the total period are different from Table 3 as these are calculated for a different period. Here periods covered for GONG and MDI are same in all activity periods. Missing values of KPMI and He I for *Phase III* are due to the unavailability of activity measurements.

Activity Index	Data Source	Phase I	Phase II	Phase III	Total
R_I	GONG	$8.56 \times 10^{-4} \pm 4.27 \times 10^{-5}$	$5.72 \times 10^{-4} \pm 1.12 \times 10^{-4}$	$9.26 \times 10^{-4} \pm 3.74 \times 10^{-5}$	$9.07 \times 10^{-4} \pm 1.74 \times 10^{-5}$
	MDI	$6.66 \times 10^{-4} \pm 7.39 \times 10^{-5}$	$5.56 \times 10^{-4} \pm 1.62 \times 10^{-4}$	$8.82 \times 10^{-4} \pm 9.43 \times 10^{-5}$	$8.35 \times 10^{-4} \pm 3.17 \times 10^{-5}$
KPMI	GONG	$8.56 \times 10^{-3} \pm 2.72 \times 10^{-4}$	$8.69 \times 10^{-3} \pm 9.49 \times 10^{-4}$	-	$8.77 \times 10^{-3} \pm 1.66 \times 10^{-4}$
	MDI	$7.40 \times 10^{-3} \pm 8.19 \times 10^{-4}$	$7.96 \times 10^{-3} \pm 1.68 \times 10^{-4}$	-	$8.06 \times 10^{-3} \pm 3.35 \times 10^{-4}$
MWSI	GONG	$2.63 \times 10^{-1} \pm 1.33 \times 10^{-2}$	$7.65 \times 10^{-2} \pm 1.57 \times 10^{-2}$	$1.68 \times 10^{-1} \pm 7.99 \times 10^{-3}$	$1.79 \times 10^{-1} \pm 5.86 \times 10^{-3}$
	MDI	$2.19 \times 10^{-1} \pm 1.95 \times 10^{-2}$	$8.28 \times 10^{-2} \pm 2.14 \times 10^{-2}$	$1.59 \times 10^{-1} \pm 1.98 \times 10^{-2}$	$1.66 \times 10^{-1} \pm 7.97 \times 10^{-3}$
F_{10}	GONG	$9.34 \times 10^{-4} \pm 3.10 \times 10^{-5}$	$6.27 \times 10^{-4} \pm 3.24 \times 10^{-5}$	$9.54 \times 10^{-4} \pm 2.34 \times 10^{-5}$	$8.71 \times 10^{-4} \pm 1.12 \times 10^{-5}$
	MDI	$7.82 \times 10^{-4} \pm 6.32 \times 10^{-5}$	$6.16 \times 10^{-4} \pm 7.71 \times 10^{-5}$	$9.51 \times 10^{-4} \pm 7.29 \times 10^{-5}$	$8.10 \times 10^{-4} \pm 2.16 \times 10^{-5}$
He I	GONG	$2.99 \times 10^{-3} \pm 1.57 \times 10^{-4}$	$1.52 \times 10^{-3} \pm 2.96 \times 10^{-4}$	-	$2.88 \times 10^{-3} \pm 9.80 \times 10^{-5}$
	MDI	$2.57 \times 10^{-3} \pm 2.89 \times 10^{-4}$	$1.58 \times 10^{-3} \pm 4.71 \times 10^{-4}$	-	$2.69 \times 10^{-3} \pm 1.45 \times 10^{-4}$
MPSI	GONG	$4.61 \times 10^{-2} \pm 1.42 \times 10^{-3}$	$2.44 \times 10^{-2} \pm 2.65 \times 10^{-3}$	$4.16 \times 10^{-2} \pm 9.54 \times 10^{-4}$	$3.96 \times 10^{-2} \pm 7.92 \times 10^{-4}$
	MDI	$4.02 \times 10^{-2} \pm 3.40 \times 10^{-3}$	$2.31 \times 10^{-2} \pm 4.48 \times 10^{-3}$	$4.15 \times 10^{-2} \pm 2.32 \times 10^{-3}$	$3.69 \times 10^{-2} \pm 1.21 \times 10^{-3}$
Mg II	GONG	$7.14 \pm 2.15 \times 10^{-1}$	$4.31 \pm 4.98 \times 10^{-1}$	$8.03 \pm 2.06 \times 10^{-1}$	$7.10 \pm 2.15 \times 10^{-1}$
	MDI	$6.08 \pm 5.13 \times 10^{-1}$	$4.06 \pm 9.23 \times 10^{-1}$	$7.93 \pm 5.25 \times 10^{-1}$	$6.60 \pm 3.14 \times 10^{-1}$
TSI	GONG	$9.47 \times 10^{-2} \pm 6.12 \times 10^{-3}$	$1.50 \times 10^{-2} \pm 7.60 \times 10^{-3}$	$7.48 \times 10^{-2} \pm 6.81 \times 10^{-3}$	$8.03 \times 10^{-2} \pm 3.74 \times 10^{-3}$
	MDI	$8.03 \times 10^{-2} \pm 1.26 \times 10^{-2}$	$1.56 \times 10^{-2} \pm 1.18 \times 10^{-2}$	$6.94 \times 10^{-2} \pm 8.91 \times 10^{-3}$	$7.52 \times 10^{-2} \pm 5.26 \times 10^{-3}$
CI	GONG	$9.46 \times 10^{-3} \pm 4.78 \times 10^{-4}$	$7.87 \times 10^{-3} \pm 1.10 \times 10^{-4}$	$9.33 \times 10^{-3} \pm 2.47 \times 10^{-3}$	$1.21 \times 10^{-2} \pm 3.92 \times 10^{-4}$
	MDI	$7.95 \times 10^{-3} \pm 8.44 \times 10^{-4}$	$6.65 \times 10^{-3} \pm 1.97 \times 10^{-4}$	$1.04 \times 10^{-2} \pm 3.01 \times 10^{-3}$	$1.11 \times 10^{-2} \pm 6.18 \times 10^{-4}$

Table 5. The correlation statistics between phase-wise correlation coefficients and slopes ($r_P([r_P(I, \delta\nu)], [b])$), and solar activity ($r_P([r_P(I, \delta\nu)], [I])$) for different activity indicators using GONG and MDI data sets.

Activity Index	$r_P([r_P(I, \delta\nu)], [b])$		$r_P([r_P(I, \delta\nu)], [I])$	
	GONG	MDI	GONG	MDI
R_I	0.98	0.74	-0.92	-0.85
KPMI	0.90	0.74	-0.85	-0.77
MWSI	0.85	0.94	-0.95	-0.85
F_{10}	0.93	0.87	-0.89	-0.72
He I	0.99	0.99	-0.85	-0.82
MPSI	0.97	0.97	-0.96	-0.92
Mg II	0.87	0.97	-0.98	-0.95
TSI	0.99	0.99	-0.85	-0.87
CI	0.47	0.34	-0.05	-0.53

Table 6. Calculated variance for different regression models using GONG frequency shifts ($\delta\nu$) and activity indices (F_{10} , MPSI and MWSI) for different phases of the solar cycle.

The coefficients A , B and C are determined from the multiple linear regression fit.

Regression Model	Total	Phase I	Phase II	Phase III
$\delta\nu = A + BF_{10}$	0.99	0.98	0.96	0.99
$\delta\nu = A + B$ (MPSI+MWSI)	0.97	0.99	0.92	0.99
$\delta\nu = A + B$ MPSI+ C MWSI	0.97	0.99	0.93	0.99
$\delta\nu = A + B$ MPSI	0.96	0.99	0.77	0.98
$\delta\nu = A + B$ MWSI	0.90	0.93	0.47	0.84